Molecular Vision 2016; 22:1280-1290 <http://www.molvis.org/molvis/v22/1280>
Received 23 July 2016 | Accepted 24 October 2016 | Published 26 October 2016

Peptide redesign for inhibition of the complement system: Targeting age-related macular degeneration

Rohith R. Mohan,[1] Andrea P. Cabrera,[1] Reed E. S. Harrison,[1] Ronald D. Gorham Jr.,[1] Lincoln V. Johnson,[2] Kaustabh Ghosh,[1] Dimitrios Morikis[1]

(The first two authors contributed equally to this work.)

[1]Department of Bioengineering, University of California, Riverside, CA; [2]Center for the Study of Macular Degeneration, Neuroscience Research Institute, University of California, Santa Barbara, CA

Purpose: To redesign a complement-inhibiting peptide with the potential to become a therapeutic for dry and wet age-related macular degeneration (AMD).
Methods: We present a new potent peptide (Peptide 2) of the compstatin family. The peptide is developed by rational design, based on a mechanistic binding hypothesis, and structural and physicochemical properties derived from molecular dynamics (MD) simulation. The inhibitory activity, efficacy, and solubility of Peptide 2 are evaluated using a hemolytic assay, a human RPE cell–based assay, and ultraviolet (UV) absorption properties, respectively, and compared to the respective properties of its parent peptide (Peptide 1).
Results: The sequence of Peptide 2 contains an arginine-serine N-terminal extension (a characteristic of parent Peptide 1) and a novel 8-polyethylene glycol (PEG) block C-terminal extension. Peptide 2 has significantly improved aqueous solubility compared to Peptide 1 and comparable complement inhibitory activity. In addition, Peptide 2 is more efficacious in inhibiting complement activation in a cell-based model that mimics the pathobiology of dry AMD.
Conclusions: We have designed a new peptide analog of compstatin that combines N-terminal polar amino acid extensions and C-terminal PEGylation extensions. This peptide demonstrates significantly improved aqueous solubility and complement inhibitory efficacy, compared to the parent peptide. The new peptide overcomes the aggregation limitation for clinical translation of previous compstatin analogs and is a candidate to become a therapeutic for the treatment of AMD.

The complement system has been implicated as a major factor in the development and progression of age-related macular degeneration (AMD) [1,2]. Genome-wide associated studies (GWASs) have shown that single nucleotide polymorphisms (SNPs) in complement regulators Factor H and Factor I and complement proteins C3, C2, and Factor B are genetic risk factors for AMD [2-4]. An important GWAS finding is the Y402H SNP of Factor H, in which a tyrosine in position 402 is replaced by a histidine, resulting in the H402 risk variant [5-8]. It has been hypothesized that in the presence of the risk variant the complement system is under-regulated, thus contributing to inflammation when activated locally in association with drusen deposits at the RPE-Bruch's membrane interface [4,9]. Although drusen formation, a characteristic accumulation of protein and membranous debris in AMD tissues, may not be initiated by the complement system, an over-activated (under-regulated) complement system has been shown to contribute to drusen accumulation and exacerbation of AMD pathology [4,10]. Therefore, inhibition of the complement system is a promising strategy to slow the progression of AMD pathogenesis.

Currently, AMD is treated using monoclonal antibody–based therapies targeting vascular endothelial growth factor (VEGF), which stimulates choroidal neovascularization and induces vascular leakage [11]. However, such therapies are effective in the wet (neovascular) form of AMD, associated with vessel rupture and local bleeding, but not in dry (atrophic) form of AMD that is characterized by the accumulation of drusen deposits and RPE atrophy. Compstatin family peptides were initially developed as inhibitors of complement-mediated autoimmune and inflammatory diseases, using phage display, functional, structural, computational studies (see review [12], and references therein). They became attractive low-molecular mass complement inhibitors for the treatment of AMD soon after the 2005 genomics studies implicated complement in AMD (see review [13], and references therein). Compstatin family peptides function by binding to complement protein C3 and sterically inhibiting the cleavage of C3 to C3a and C3b by convertase, thus impeding the formation of the chemotactic fragment

Correspondence to: Dimitrios Morikis, Department of Bioengineering, University of California, Riverside, CA, 92521; Phone: (951) 827-2696; FAX: (951) 827-6416; email: dmorikis@ucr.edu

Table 1. Peptide sequences.

Peptide	Sequence	Molecular mass
1	Ac- RSI[CVWQDWGAHRC]T -NH_2	1856
2	Ac- RSI[CVWQDWGAHRC]T-PEG_8 -NH_2	2279

Peptide 1 is a positive control with a two-polar amino acid N-terminal extension [22]. Peptide 2 is a new design that contains an 8-PEG block backbone extension. Brackets denote disulfide bridge cyclization between the two cysteine amino acids. Ac: acetylation blocking group; NH_2: amidation blocking group.

C3a, the opsoninizing fragment C3b, and the propagation of the complement system through the common pathway that ultimately results in the assembly of C5b-9_n (also known as the membrane attack complex, MAC), a protein complex that forms pores on cell membranes.

One compstatin analog underwent clinical trials for AMD, and although the analog did not raise safety concerns, it did not show therapeutic efficacy. It is postulated that was likely the effects of molecular aggregation that resulted in the formation of gel-like structures [14,15] and an associated loss of functionality. This analog had been optimized over several years to have higher binding affinity than the original compstatin analogs by introducing a replacement of valine at position 4 with an aromatic amino acid, tyrosine [16,17] or tryptophan [18], and subsequently with methylated tryptophan [19]. The latter modification also increased the hydrophobic character of the peptide and presumably contributed to its aggregation in the aqueous ocular environment. Additional compstatin analogs are currently in clinical trials for various complement-mediated diseases [20].

Recent studies have focused on increasing the solubility of compstatin peptides, using structure-based rational design, computational modeling, and optimization [21,22]. These studies have identified several analogs with N-terminal extensions that have inhibitory activities similar to those of the most potent analogs and have higher aqueous solubilities. Increased solubility was made possible by introducing two polar amino acid extensions at the N-terminus. In one analog, an arginine at sequence position −1 not only contributed to solubility but was also shown by molecular dynamics simulations to form a salt bridge with a glutamic acid in C3, thus contributing to binding affinity as well [21,22]. In this study, we used a potent analog with arginine at position −1 and serine at position 0 [22], Peptide 1 here (or Peptide 9 in [22]), as a template to further increase solubility by incorporating two polar amino acid extensions and polyethylene glycol (PEG) blocks at the C-terminus. We demonstrate the high potency and high solubility of the new analog, using in vitro functional and solubility assays. We also demonstrate the efficacy of this peptide to inhibit complement activation in a human RPE cell–based assay that mimics AMD pathophysiology. We show that this PEGylated compstatin analog has significant promise as a therapeutic for AMD.

METHODS

Peptide synthesis: Compstatin Peptides 1 and 2 (Table 1) were synthesized by WuXi AppTec (Shanghai, China). Peptide 2 has eight PEG blocks attached at the backbone of the C-terminal amino acid. Both peptides were cyclized by a disulfide bridge between the two cysteine amino acids, and they were acetylated at the N-terminus and amidated at the C-terminus. The peptides had >95% purity, as determined with high-performance liquid chromatography (HPLC) and mass spectrometry (MS).

Hemolytic assay: Rabbit erythrocytes (Complement Technology, Inc., Tyler, TX) were washed with PBS (1X; 3.8 mM monobasic NaH_2PO_4, 16.2 mM dibasic Na_2HPO_4, 150 mM NaCl, pH 7.4) and then resuspended in a veronal-buffered saline solution (VBS 1X; 72.8 mM NaCl, 0.9 mM sodium barbital, 1.5 mM barbituric acid, pH 7.4) containing 5 mM $MgCl_2$ and 10 mM EGTA (VBS-MgEGTA). Twofold serial dilutions of the compstatin analogs were performed in round-bottom 96-well plates and then further diluted in VBS-MgEGTA. Normal human serum (NHS; Complement Technology, Inc.) diluted in VBS-MgEGTA was added to each well followed by incubation at room temperature for 15 min. Subsequently, 30 µl of rabbit erythrocytes at a concentration of 1.25×10^8 cells/ml were added to each well. Positive controls for lysis consisted of erythrocytes in deionized water and erythrocytes in NHS diluted with VBS-MgEGTA. Negative controls for lysis consisted of erythrocytes in VBS-MgEGTA and erythrocytes in NHS diluted in VBS-EDTA (20 mM EDTA). Next, plates were incubated at 37 °C for 20 min, and then ice-cold VBS containing 50 mM EDTA was added to each well to quench hemolytic reactions. The plates were centrifuged at 1000 ×*g* for 5 min, and the supernatant was diluted 1:1 with deionized water in flat-bottom 96-well plates. Absorbance was measured spectrophotometrically at 405 nm to quantify lysis.

Apparent solubility measurements: Compstatin analogs were dissolved in PBS at pH 7.4 to concentrations of 10, 7.5, and 5 mg/ml. At each concentration point, the peptide solutions were shaken on a vortex mixer for 30 s and then centrifuged at 13,000 ×*g* for 5 min. The supernatant was collected and measured 5 times spectrophotometrically at 280 nm. Optical densities were converted into concentrations according to the Beer-Lambert law. An extinction coefficient of 11,125 M^{-1} cm^{-1} was used for each compstatin analog as each peptide contains two tryptophan amino acids (tryptophan extinction coefficient being 5562.5 M^{-1} cm^{-1}).

RPE cell culture: The in vitro model of drusen biogenesis was used as previously reported [23] and used in assessing the efficacy of compstatin peptides [21,22]. Briefly, RPE cells from human fetal eyes, obtained as previously described [24], were used within the second passage were grown on laminin-coated porous inserts (Millipore, Billerica, MA) in Miller medium [25] supplemented with 5% fetal bovine serum (FBS; HyClone, Logan, UT) at 37 °C and 5% CO_2 in a humidified incubator. After culturing for 2–3 months, the cells were rinsed with PBS and treated with Miller medium containing either 5% FBS (negative control) or 10% NHS without or with the inhibitory peptides (2 µM). The choice of the 2 µM dose for this assay was based on the intent to use double the IC_{50} concentration, which was determined to be about 1 µM. All inhibitory peptides were premixed with NHS on a rocker at room temperature for 30 min and then warmed to 37 °C before being added to the RPE cell cultures for 24 h. Next, the cells were rinsed with PBS, fixed in 4% paraformaldehyde (PFA; Electron Microscopy Sciences, Hatfield, PA) for 20 min, and stored in 0.4% PFA until use in the immunofluorescence assays.

Immunofluorescence of sub-RPE deposits: Basal deposits formed by the RPE cultures were visualized with immunofluorescence, as previously described [21,23]. Briefly, porous inserts were excised with a scalpel, cut into approximate 4 mm^2 pieces, and rinsed several times with PBS. Next, one half of all RPE culture inserts were embedded in 10% (w/v) agarose (Fisher, Waltham, MA) and sectioned at 100 µm using a vibratome, while the other half was subjected to decellularization (to remove the RPE monolayer) using our previously reported protocol [26,27]. Briefly, to obtain decellularized inserts, confluent RPE monolayers were incubated in Ca^{2+}, Mg^{2+}-free PBS for 30 min before treatment with a mild detergent composed of 1% Triton X-100 and 80 mM ammonium hydroxide for 5 min. The decellularized inserts were next rinsed in PBS three times before fixation with 4% PFA (20 min). Next, the vibratome sections and decellularized inserts were blocked with 5% donkey serum in PBS containing 0.5% BSA and 0.1% Triton X-100 (overnight at 4 °C) and labeled with mouse anti-C5b-9 (AbCam, Cambridge, MA; overnight at 4 °C or 2 h at room temperature), followed by labeling (2 h at room temperature) with Alexa Fluor 488-labeled anti-mouse immunoglobulin G (IgG; Life Technologies, Carlsbad, CA). The immunolabeled decellularized inserts were directly mounted in Fluoromount (Sigma, St. Louis, MO) while the sections were counterstained with 4',6-diamidino-2-phenylindole (DAPI), a nuclear stain, before mounting.

Confocal imaging and analysis: Immunolabeled RPE sections and decellularized culture inserts were imaged using a Leica (Leica Microsystems, Buffalo Grove, IL) SP5 confocal microscope. Single-plane images from multiple non-overlapping areas were acquired using a 63× objective, and C5b-9_n (MAC) immunofluorescence signals were quantified using ImageJ (National Institute of Health, Bethesda, MD), as we have previously reported [21]. Briefly, the color thresholding tool of ImageJ was used to analyze the intensity of C5b-9n associated fluorescence. Here, the upper intensity threshold was set such that the entire deposit area was selected for fluorescence intensity measurement while the lower intensity threshold was set to eliminate any background fluorescence. For statistical analysis, fluorescence intensity measurements of C5b-9n were averaged from multiple images and normalized with respect to the number of RPE nuclei per image (for vibratome sections) or the total image area (for decellularized whole mount samples) and then expressed as a percentage of the corresponding fluorescence intensities from samples exposed to NHS in the absence of any inhibitory peptide (positive control). All data were obtained from multiple images ($n \geq 9$) of fhRPE cells from the same donor and expressed as mean ± standard error of the mean (SEM). Statistical significance was determined using ANOVA (ANOVA), followed by Tukey's post-hoc analysis (Instat GraphPad Software Inc., La Jolla, CA). A p value of less than 0.05 was considered statistically significant.

Structural modeling: A structural model of the eight-linked PEG blocks was generated using MOLDRAW [28] and then attached to a structural model of Peptide 1 using structure editing tools in Chimera [29], to generate a structural model of Peptide 2. The structural model of Peptide 1 was derived from molecular dynamics simulations, based on the crystal structure of bound compstatin [30]. CHARMM parameters and topologies [31] were used and modified to incorporate the peptide-like bond between PEG_8 and Peptide 1. Modifications were rationally chosen based on existing amino acid parameters and topologies. Angles and dihedral angles that did not have a counterpart in existing CHARMM parameters and topologies were generated using SwissParam [32].

Molecular dynamics simulation: An explicit-solvent molecular dynamics simulation was performed, for 90 ns, using as the initial structure the modeled Peptide 2 structure. The explicit-solvent environment consisted of a water box and counterions to represent the solvated environment of the biomolecular system. The peptide was solvated in a TIP3P water box with dimensions of 75 × 57 × 67 Å, and charges were neutralized with sodium and chloride counterions at 150 mM. The TIP3P water model is a standard 3-site water model used in explicit solvent MD simulations that describes the configuration of the water molecules (rigidity/flexibility), polarization, and interactions in the simulation. Preparation steps (minimization, heating, and equilibration) were carried out to remove strain in the system, to heat the system to the desired temperature, and to relax the system prior to the production simulation dynamics, as described in a previous study [33]. Following 25,000 steps of conjugate gradient energy minimization, the system was heated from 0 to 300 K in 62 ps with protein atoms constrained to post-minimization positions. Subsequently, the system was equilibrated through five stages for 50 ps per stage. Force constants of 41.83, 20.92, 8.368, and 4.184 kJ/mol/Å^2 were applied during the first four stages, respectively, to harmonically constrain all protein atoms to their post-minimization positions. During the fifth stage of equilibration, only the backbone atoms were harmonically constrained using a force constant of 4.184 kJ/mol/Å^2. Following equilibration, a production run was performed for 90 ns with periodic boundary conditions, SHAKE algorithm, 2 fs time steps, Langevin pressure and temperature controls, and particle-mesh Ewald electrostatics. The molecular dynamics trajectory (9,000 frames) was clustered using the root-mean-square deviation (RMSD) of the backbone or alpha carbon atoms of Peptide 2, and a representative structure from the highest-populated clusters was identified and depicted for molecular graphics visualization.

RESULTS

The objective of this study is to optimize the aqueous solubility while maintaining the binding affinity of Peptide 1 (Table 1), our compstatin peptide that previously had the most promise to become a therapeutic for AMD. Our previous studies [21,22] focused on improving the solubility of the peptide that underwent clinical studies for AMD, with sequence Ac-I[CV(meW)QDWGAHRC]T-NH_2 [13]. This peptide had high aggregation propensity in aqueous solution, attributed to the peptide's reduced solubility compared to other less potent compstatin analogs [21]. It was first shown that adding polar dipeptides at the N-terminus (positions −1 and 0) improved solubility while maintaining potency, with the peptide Ac-RSI[CV(meW)QDWGAHRC]T-NH_2 was the most efficacious in the human RPE cell–based assay described in Methods (Peptide VI in [21]). In a subsequent study, it was deemed necessary to eliminate the methyl group from tryptophan at position 4 to further improve solubility, without compromising potency, resulting in the sequence of Peptide 1 (Peptide 9 in [22]).

To achieve our objective, we redesigned Peptide 1 by adding PEG block extensions at the C-terminus (Peptide 2; Table 1). The choice of the extension at the C-terminus of Peptide 2 was guided by the results of molecular dynamics simulations, which had shown that the C-terminus of compstatin points away from the C3-binding site toward the solvent [21,34]. Thus, we reasoned that such extensions would not interfere with the binding interface between the compstatin analog and C3. Peptide 2 contains eight PEG blocks attached at the peptide backbone in the C-terminus. The choice of PEG blocks was guided by earlier surface plasmon resonance (SPR) and enzyme-linked immunosorbent assay (ELISA) data, which had shown that PEGylated compstatin peptides had higher solubility compared to non-PEGylated peptides with the same sequence [35]. The addition of a spacer of eight PEG blocks to compstatin analogs was deemed necessary for the SPR binding experiments to increase the space between the peptides and attachment to the streptavidin sensor chip via lysine–biotin binding. This spacer aimed to increase the mobility of the peptides, enhance their accessibility to C3, and decrease non-specific interactions, thus emulating unbound ligand states as closely as possible within the experimental constraints. The inhibitory activities of peptides with the same sequences, but without the PEG blocks, were tested using ELISAs in the same study [35]. PEGylation is an established procedure in drug design and delivery, as this procedure has been shown to increase aqueous solubility and bioavailability, including enhanced structural and chemical stability and circulation lifespan, and reduced renal clearance [36]. In addition, PEGylation has a shielding effect on drugs, typically reducing drug immunogenicity, antigenicity, and toxicity [36]. Currently, there are several PEGylated drugs in the clinic, including pegaptanib, which has been used for the treatment of age-related macular degeneration [37]. PEGylation has also been used in a compstatin variant with modified backbone, but in that case, a large (40 kDa) Y-shaped PEG structure was attached either at the N- or C-terminus [38], compared to the small (423 Da) linear 8-PEG block structure attached at the C-terminus in our study.

Figure 1 shows the dose–response curves of the complement hemolytic assay for the PEGylated Peptide 2 and the parent Peptide 1 (positive control). Peptides 1 and 2 have

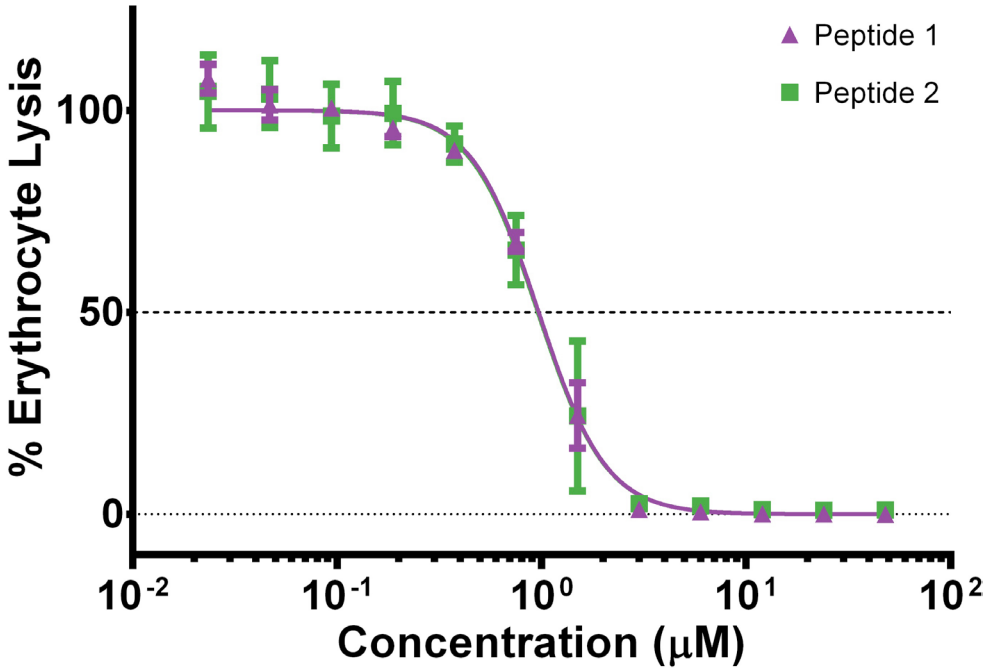

Figure 1. Concentration-dependent inhibition curves of compstatin peptides in four replicate hemolytic assay experiments. The plotted data represent the mean percent inhibition ± standard error of the mean (SEM). The dashed line intersects each inhibition curve at the IC_{50}. Peptide 1 is the parent peptide (positive control), and Peptide 2 is the PEGylated form of the parent peptide.

similar IC_{50} values within the confidence intervals from four replicate experiments, and therefore similar potencies (Table 2).

We then tested our solubility objective. Figure 2A shows the difference between the calculated and spectrophotometrically measured (observed) concentrations in the range of 5–10 mg/ml. The concentration was experimentally measured using absorption spectroscopy at 280 nm and calculated using the weight per volume values of the dilution series, as described in Methods. Peptide 2 is much more soluble than Peptide 1 at 5 mg/ml, as the concentration difference is close to zero, the expected difference for nearly perfect solubility. In addition, Peptide 2 remains soluble up to 10 mg/ml with a slight deviation from the difference of zero, whereas the difference of Peptide 1 significantly deviates from zero and from constancy as the concentration increases. Figure 2B shows a different presentation of the same data in the form of a correlation plot between the observed and calculated peptide concentrations in millimolar. The data for Peptide 2 show much higher correlation than those for Peptide 1. In addition, the fitted straight line of the data for Peptide 2 is closer to a straight line with slope 1 that passes through the origin (Figure 2B). A straight line with slope 1 represents perfect correlation, denoting the highest solubility and the lowest aggregation. These data demonstrate that Peptide 2 has significantly higher apparent solubility, or significantly lower tendency to aggregate, than the parent Peptide 1.

Table 2. IC_{50} Values from hemolytic assay.

Peptide	Mean IC_{50} (μM)	95% Confidence interval	
		Upper	Lower
1	0.97	1.04	0.90
2	0.96	1.14	0.80

IC_{50}: Ligand concentration at 50% maximal inhibition. Data are from four replicate experiments (n=4).

We continued our study by testing the efficacy of Peptides 1 and 2 in a human RPE cell–based assay [23], which was used in previous optimizations of compstatin family peptides [21,22]. This assay is based on a human RPE cell culture that mimics the pathophysiology of AMD and can be used to interrogate the effects of complement activation in AMD pathogenesis. The assay is useful for quantification of the effects of inhibitors on complement activation mediated by sub-RPE drusen-like deposits, typical of those present in early AMD. Figure 3 shows the deposition of deposit-associated C5b-9_n following the addition of NHS as a complement source [21,23]. Exposure of cell-free inserts to NHS did not show any evidence of C5b-9_n immunoreactivity (Appendix 1), indicating that the baseline level of alternative pathway activation in NHS does not likely contribute to this increased accumulation of sub-C5b-9_n. Confocal imaging of immunolabeled RPE culture sections (Figure 3) and (decellularized) whole mounts (Appendix 2) revealed that deposit-associated sub-RPE C5b-9_n deposition is inhibited by both compstatin peptides. More specifically, quantification of

anti-C5b-9 immunofluorescence from whole mounts revealed that Peptide 2 causes a remarkable 80% inhibition ($p<0.001$) of complement activation (Figure 4). The inhibitory effect of Peptide 2 was significantly greater ($p<0.001$) than that achieved by Peptide 1, which reduced C5b-9_n deposition to a lesser degree (50%; $p<0.001$).

In combination, the hemolytic assay, apparent solubility, and human RPE cell–based assay data indicate that Peptide 2 is a more promising compstatin analog for further optimization and potential clinical translation, compared to Peptide 1. The parent Peptide 1 had emerged to be the best analog until now in previous studies, in terms of solubility and affinity balance and efficacy of complement inhibition in the human RPE cell–based assay (see [21,22] and references therein for earlier optimization studies).

To gain insight into the molecular features that contribute to the structural stability and solubility of Peptide 2, we performed an extended molecular dynamics simulation. Figure 5A shows representative conformations from the top (highest occupancy) five structural clusters derived from the molecular dynamics trajectory, using backbone atom RMSD-based clustering. These five clusters represent 79% of the conformations spanned by the peptide. The PEG_8 C-terminal extension demonstrates high local flexibility and global mobility, in essence forming a dynamic polar shell around Peptide 2. Flexibility and mobility of the PEG_8 extension are expected, given its polar character and interactions with water molecules of the solvent. This dynamic polar shell perhaps functions as a shield from self-association and aggregation of Peptide 2 owed to peptide's inherent hydrophobic features, thus contributing to the solubility of the peptide.

Figure 5B shows the conformation of the representative peptide from the structural cluster with highest occupancy, depicting key amino acid side chains for the optimization of compstatin from research in the past 20 years. These amino acids are Arg(-1), Val3, Trp4, Trp7, Ala9, and the disulfide bridge Cys2-Cys12. The Arg(-1) addition corresponds to the Arg(-1)/Ser0 extension of Peptide 1 [22], the parent analog of Peptide 2. Our latest addition in this work is the PEG_8-NH_2 (Figure 5D) extension at the C-terminus (Figure 5A–C), which results in Peptide 2, our most promising, in terms of affinity and solubility properties, lead peptide of the compstatin family until now.

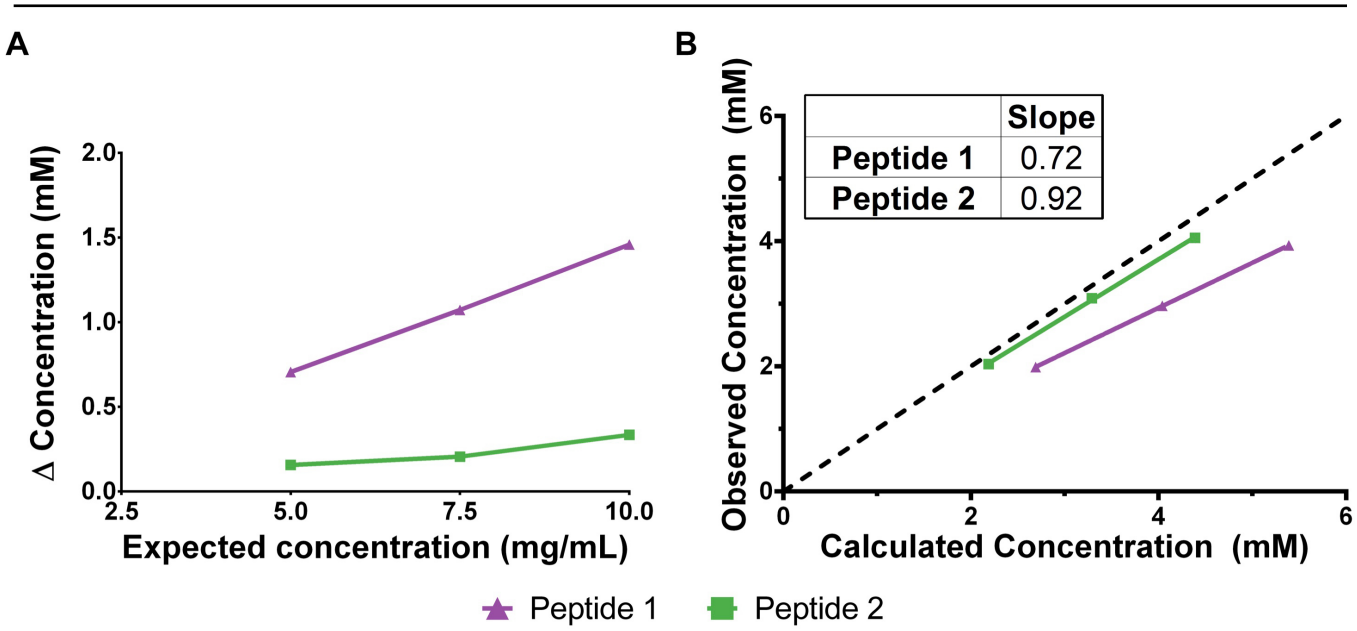

Figure 2. Apparent solubility of compstatin peptides. **A**: The difference in concentration, calculated – observed (measured), in mM, plotted against the expected concentration (in mg/ml). The actual observables are plotted, the expected concentration (in mg/ml) of the dilution series on the horizontal axis, and the observed (in mM, measured using tryptophan absorbance) minus the calculated (in mM, from the mg/ml expected concentration values) on the vertical axis. Peptide 2 is the most soluble, as the concentration difference is close to zero and remains nearly constant in the dilution series. **B**: Correlation of the observed concentration with the calculated concentration, with the concentrations presented in mM. Peptide 2 is the most soluble, as indicated by the high correlation between the observed and calculated concentrations (slope of 0.92). Each data point represents the mean measured concentration and the corresponding expected concentration with a linear regression fit to the data. A straight line of slope 1 passing through the origin is inserted to indicate the closeness of the data to perfect correlation.

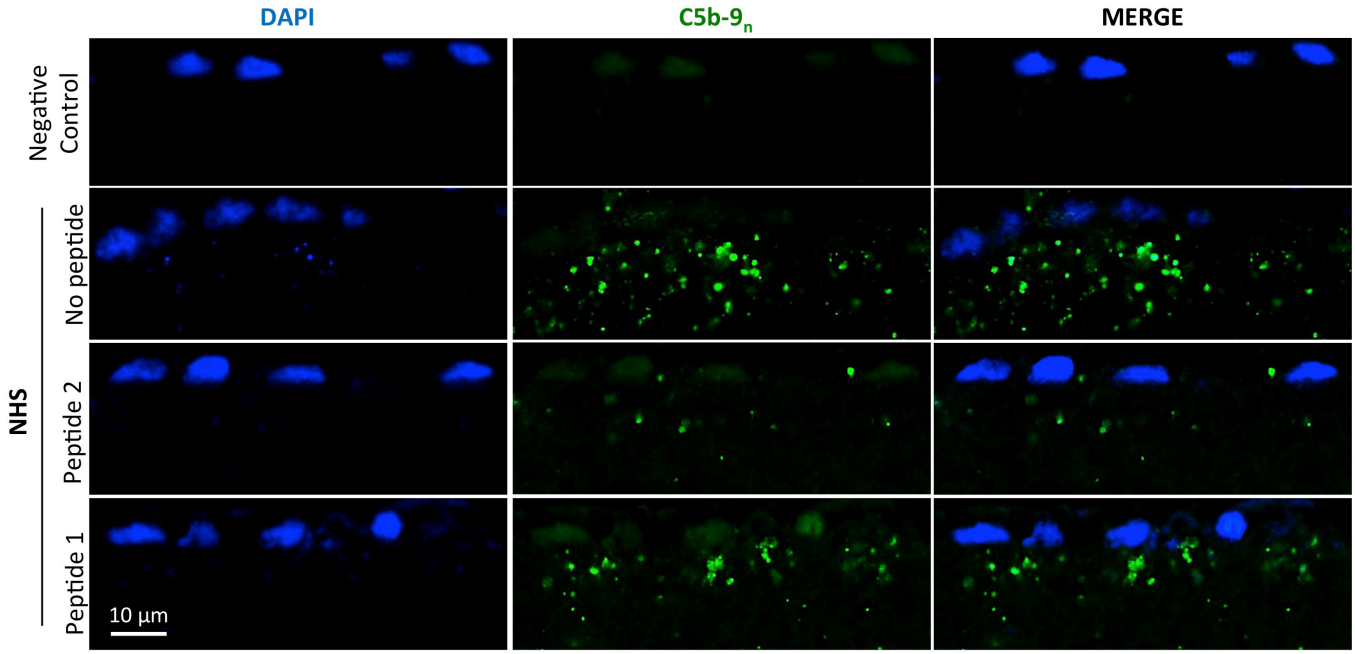

Figure 3. Human RPE cells form basal deposits rich in C5b-9$_n$ (MAC) in vitro, and inhibitory effects of compstatin peptides. Representative cross-sectional images show 3-month-old RPE cell cultures labeled with anti-C5b-9$_n$ (green) and 4',6-diamidino-2-phenylindole (DAPI; blue), following exposure to either 10% normal human serum (NHS) alone or together with Peptides 1 and 2 for 24 h. Cultures that received no NHS treatment served as negative control. Scale bar = 10 µm.

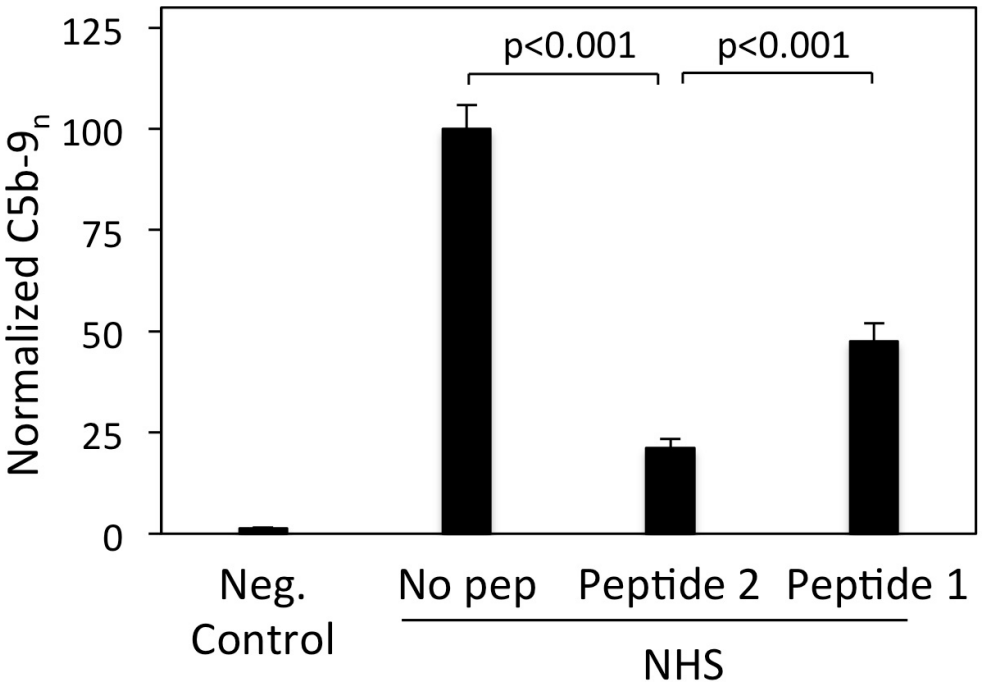

Figure 4. Compstatin peptides inhibit complement-induced C5b-9$_n$ deposition in RPE culture. Fluorescence intensity measurements from anti-C5b-9$_n$-labeled (decellularized) whole mount samples ($n \geq 9$) were normalized human serum (NHS)-treated samples and plotted as mean ± standard error of the mean (SEM). Data analyses show that Peptide 2 causes 80% reduction in NHS-induced basal C5b-9$_n$ deposition by RPE cells. Peptide 1 exhibits a weaker inhibitory effect, reducing C5b-9$_n$ deposition by 50%. Bars indicate mean ± SEM.

DISCUSSION

We report the design of a new compstatin peptide that has superior aqueous solubility and comparable complement inhibitory activity characteristics, compared to previously known peptides of the compstatin family. The new peptide, Peptide 2 (Table 1), is a PEGylated form of our previously most promising peptide in terms of inhibitory activity and aqueous solubility, Peptide 1 (Table 1) [22]. Peptide 2 has eight PEG blocks attached to the backbone C-terminus, accounting for an additional molecular mass of 423 Da compared to Peptide 1 (Table 1). Since the original discovery of compstatin using a phage-displayed random peptide library [39], there have been many benchmarks in the optimization of the sequence of compstatin. Initial structure-activity studies had derived a sequence template with seven amino acids being indispensable for inhibitory activity and six amino acids being optimizable [17,40]. Figure 5B shows the side chains of essential amino acids for the optimal binding and inhibitory activity of compstatin, including benchmark residue-specific optimization steps over the period of several years. Initial NMR, alanine scan, and inhibitory activity studies indicated that Val3 and Trp7 are important for binding to C3 and inhibition of complement activation [41,42]. A subsequent crystal structure of C3c in complex with a compstatin analog confirmed these findings, showing that Val3 and Trp7 are inserted in hydrophobic cavities [30]. Benchmark optimization steps include the incorporation of (i) Ala at position 9, which introduces helicity in the sequence and shifts a structural beta-turn from the central toward the C-terminal portion of the sequence [41,42]; (ii) aromatic amino acids at position 4 [16] with Trp4 being optimal [18], which was shown to participate in a hydrophobic clustering in the crystal structure [30]; (iii) dipeptide N-terminal extensions, with Arg at position −1 being optimal because it increased solubility compared to previous peptides and introduced a new intermolecular salt bridge as shown by molecular dynamics simulations [21,22]; and in this work, (iv) C-terminal extension using an eight-block PEG construct, which greatly increases aqueous solubility, unprecedented by any other compstatin analog. In

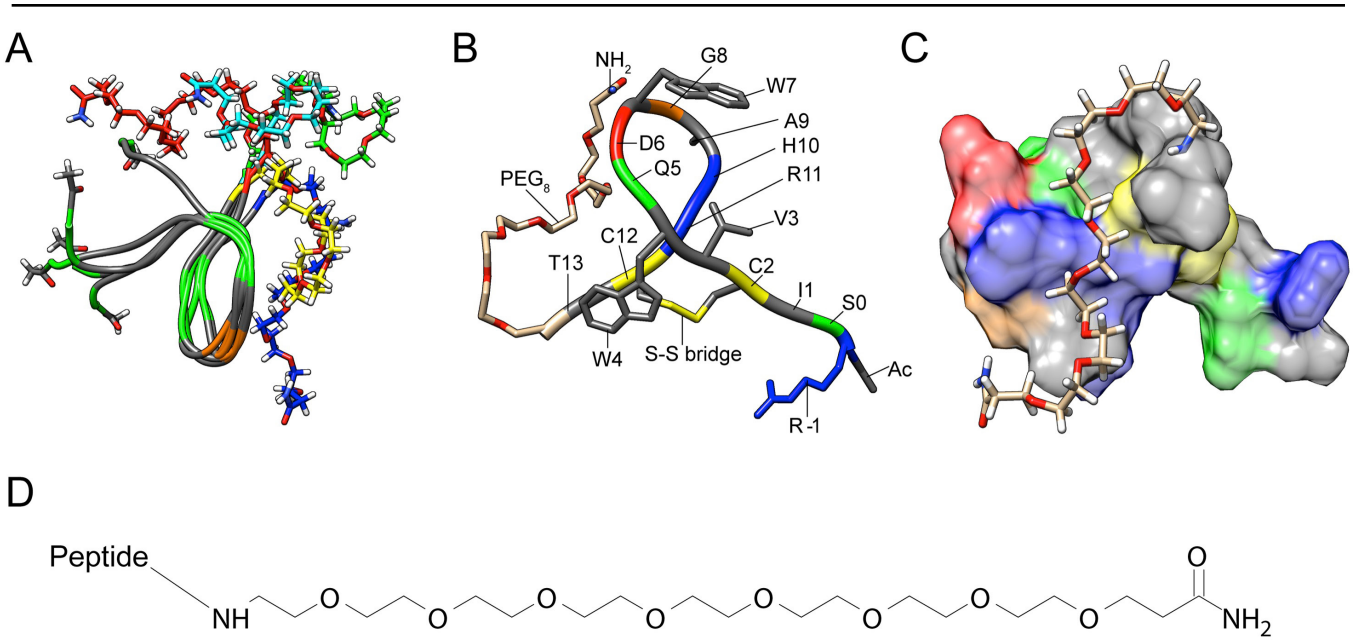

Figure 5. Molecular structure of Peptide 2. **A**: Representative conformers of Peptide 2 from the five highest-populated root-mean-square deviation (RMSD) clusters of the molecular dynamics trajectory, with occupancies of 38%, 12%, 10%, 10%, and 9%. The peptide backbone is shown in a tube representation, colored by the amino acid property type: gray for hydrophobic, green for polar, and brown for glycine. Cys2 and Cys12 are marked as hydrophobic because they form a disulfide bridge. The PEG_8 C-terminal extensions are shown in stick models of different colors for each conformer. The acetyl and amide terminal blocks are shown in stick models, colored by atom type: gray for carbon, white for hydrogen, blue for nitrogen, and red for oxygen. **B**: The major conformer of Peptide 2 (38% occupancy) in backbone tube representation, with key side chains in compstatin peptide optimization in stick representation. The location of all amino acids is marked. The following color code is used: gray for hydrophobic, green for polar neutral, blue for basic, red for acidic, yellow for cysteines and the disulfide bridge, and brown for glycine. The PEG_8-NH_2 C-terminal extension is shown in stick representation without hydrogens, with carbons depicted in brown, oxygens in red, and nitrogen in blue. **C**: Surface representation of Peptide 2, with the PEG_8-NH_2 extension shown in stick representation (including hydrogens). The color code is as in Panel **B**, with the added hydrogens of PEG_8-NH_2 shown in white. **D**: The chemical structure of PEG_8-NH_2.

addition, acetylation at the N-terminus and amidation at the C-terminus contribute to improved activity [43]. All active peptides contain a Cys2-Cys12 disulfide bridge.

Compstatin has two surfaces, a hydrophobic and a polar one, as was pointed out by the original NMR studies [41,42], but it is the hydrophobic surface that makes the main contacts with the C3, as it was pointed out by the crystal structure [30]. It is likely that the hydrophobic surface is responsible for the aggregation properties of the compstatin analog that underwent the early clinical trials. This analog contained a methylated Trp4 residue, in which the hydrophobic methyl group had replaced the polar hydrogen of the indole amide group, making the peptide even more hydrophobic. We had reasoned in earlier optimization studies that incorporation of polar amino acid extensions at the termini would increase solubility without perturbing binding properties, and this was shown to be the case for the N-terminus [21,22] and C-terminus (Mohan RR, Gorham RD Jr, Morikis D, unpublished data). However, the analog with the best aqueous solubility is Peptide 2 of this work that incorporates an 8-PEG block construct at the C-terminus. Our earlier molecular dynamics studies had shown that the C-terminus is mobile pointing outward from the C3-peptide interface toward the solvent. Thus, we reasoned that the 8-PEG block construct would not sterically interfere with the binding interface of the C3-peptide complex. This is evident in Figure 5, where the 8-PEG construct shows mobility around the non-binding site of Peptide 2, without specific contacts with the peptide. Therefore, PEGylation acts a solubilizer of compstatin.

To determine the potential of Peptide 2 and its parent Peptide 1 as AMD therapeutics, we evaluated the peptides in the human RPE cell–based assay. As we have reported before [36], this in vitro assay is characterized by the formation of C5b-9-rich sub-RPE deposits, a hallmark of dry AMD. Thus, this assay represents a unique testbed for screening therapeutic candidates for treatment of dry AMD. We have successfully used this assay for our recent optimization studies that resulted in the incorporation of polar N-terminal extensions in our compstatin analogs [21,22]. Here, we use this assay to demonstrate that Peptides 1 and 2 significantly inhibit the formation of C5b-9-rich sub-RPE deposits, with the PEGylated Peptide 2 exhibiting a twofold greater inhibitory effect than the parent Peptide 1. This difference in anti-C5b-9 effect may be attributed to lack of aggregation of Peptide 2, owing to its greater solubility compared to Peptide 1, which is expected to result in a higher "effective" concentration in the RPE culture. At the molecular level, the optimal solubility of Peptide 2 results from the formation of a dynamic polar shell, introduced by PEGylation, which predominantly surrounds and enhances the polar surface, and to a lesser extent the nonpolar surface of the peptide. This polar shell is designed to be a solubilizer, shielding Peptide 2 from self-association and higher-order aggregation, while leaving it unobstructed for binding the nonpolar surface.

In conclusion, we report the design of a new peptide analog of compstatin that combines an arginine-serine N-terminal polar amino acid extension and an 8-PEG block C-terminal extension. This peptide demonstrates significantly improved aqueous solubility and efficacy in a human RPE cell–based assay that mimics the pathobiology of AMD, compared to its parent peptide, while retaining comparable inhibitory activity against complement activation as its parent peptide. The new peptide can lead to a therapeutic treatment of dry AMD, as the peptide overcomes the aggregation limitation of a previous compstatin analog that underwent clinical trials.

APPENDIX 1.

Representative whole-mount images show 'cell-free' culture inserts labeled with anti-C5b-9_n (green) following exposure to 10% NHS for 24h. No evidence of C5b-9_n immunoreactivity is seen in the absence of RPE cells. To access the data, click or select the words "Appendix 1."

APPENDIX 2.

Representative whole-mount images show two month-old RPE cell cultures labeled with anti-C5b-9_n (green) following exposure to either 10% NHS alone or together with peptides 1 and 2 for 24h. Cultures that received no NHS treatment served as negative control. Scale bar: 25 µm. To access the data, click or select the words "Appendix 2."

ACKNOWLEDGMENTS

DM acknowledges the donors to Macular Degeneration Research, a program of the BrightFocus Foundation, for support of this research (Grant M2013106), and the University of California, Riverside, Research and Economic Development Office for support through the Proof of Concept program. DM is the 2013 recipient of the Carolyn K. McGillvray Memorial Award for Macular Degeneration Research, administered by the Bright-Focus Foundation. KG acknowledges initial complement support from the Bourns College of Engineering of the University of California, Riverside. DM and RDG are co-inventors in patent applications of compstatin peptides, and DM, KG, RRM, APC, RESH, and RDG are co-inventors in a patent application for the PEGylated peptide described in this paper. Dimitrios Morikis

(dmorikis@ucr.edu) and Kaustabh Ghosh (kghosh@engr.ucr.edu) are co-corresponding authors for this paper.

REFERENCES

1. Liszewski MK, Atkinson JP. Complement regulators in human disease: lessons from modern genetics. J Intern Med 2015; 277:294-305. [PMID: 25495259].
2. Schramm EC, Clark SJ, Triebwasser MP, Raychaudhuri S, Seddon JM, Atkinson JP. Genetic variants in the complement system predisposing to age-related macular degeneration: A review. Mol Immunol 2014; 61:118-25. [PMID: 25034031].
3. Black JRM, Clark SJ. Age-related macular degeneration: genome-wide association studies to translation. Genet Med 2016; 18:283-9. [PMID: 26020418].
4. Anderson DH, Radeke MJ, Gallo NB, Chapin EA, Johnson PT, Curletti CR, Hancox LS, Hu J, Ebright JN, Malek G, Hauser MA, Rickman CB, Bok D, Hageman GS, Johnson LV. The pivotal role of the complement system in aging and age-related macular degeneration: Hypothesis re-visited. Prog Retin Eye Res 2010; 29:95-112. [PMID: 19961953].
5. Hageman GS, Anderson DH, Johnson LV, Hancox LS, Taiber AJ, Hardisty LI, Hageman JL, Stockman HA, Borchardt JD, Gehrs KM, Smith RJH, Silvestri G, Russell SR, Klaver CCW, Barbazetto I, Chang S, Yannuzzi LA, Barile GR, Merriam JC, Smith RT, Olsh AK, Bergeron J, Zernant J, Merriam JE, Gold B, Dean M, Allikmets R. A common haplotype in the complement regulatory gene factor H (HF1/CFH) predisposes individuals to age-related macular degeneration. Proc Natl Acad Sci USA 2005; 102:7227-32. [PMID: 15870199].
6. Klein RJ, Zeiss C, Chew EY, Tsai J-Y, Sackler RS, Haynes C, Henning AK, SanGiovanni JP, Mane SM, Mayne ST, Bracken MB, Ferris FL, Ott J, Barnstable C, Hoh J. Complement Factor H Polymorphism in Age-Related Macular Degeneration. Science 2005; 308:385-9. [PMID: 15761122].
7. Haines JL, Hauser MA, Schmidt S, Scott WK, Olson LM, Gallins P, Spencer KL, Kwan SY, Noureddine M, Gilbert JR, Schnetz-Boutaud N, Agarwal A, Postel EA, Pericak-Vance MA. Complement Factor H Variant Increases the Risk of Age-Related Macular Degeneration. Science 2005; 308:419-21. [PMID: 15761120].
8. Edwards AO, Ritter R, Abel KJ, Manning A, Panhuysen C, Farrer LA. Complement Factor H Polymorphism and Age-Related Macular Degeneration. Science 2005; 308:421-4. [PMID: 15761121].
9. Hollyfield JG. Age-Related Macular Degeneration: The Molecular Link between Oxidative Damage, Tissue-Specific Inflammation and Outer Retinal Disease The Proctor Lecture. Invest Ophthalmol Vis Sci 2010; 51:1276-81. [PMID: 20185837].
10. Anderson DH, Mullins RF, Hageman GS, Johnson LV. A role for local inflammation in the formation of drusen in the aging eye. Am J Ophthalmol 2002; 134:411-31. [PMID: 12208254].
11. Lai K, Landa G. Current choice of treatments for neovascular AMD. Expert Review of Clinical Pharmacology 2015; 8:135-40. [PMID: 25487081].
12. Morikis D, Lambris JD. Structure, dynamics, activity, and function of compstatin and design of more potent analogues. Structural Biology of the Complement System 2005:317–40.
13. Ricklin D, Lambris JD. Compstatin: A Complement Inhibitor on its Way to Clinical Application. In: Lambris JD, editor. Current Topics in Complement Ii. Vol 6322008. p. 273–92.
14. Zarbin MA, Rosenfeld PJ. PATHWAY-BASED THERAPIES FOR AGE-RELATED MACULAR DEGENERATION An Integrated Survey of Emerging Treatment Alternatives. Retina-the Journal of Retinal and Vitreous Diseases 2010; 30:1350-67. [PMID: 20924259].
15. Yehoshua Z, Rosenfeld PJ, Albini TA. Current Clinical Trials in Dry AMD and the Definition of Appropriate Clinical Outcome Measures. Semin Ophthalmol 2011; 26:167-80. [PMID: 21609230].
16. Klepeis JL, Floudas CA, Morikis D, Tsokos CG, Argyropoulos E, Spruce L, Lambris JD. Integrated computational and experimental approach for lead optimization and design of compstatin variants with improved activity. J Am Chem Soc 2003; 125:8422-3. [PMID: 12848533].
17. Morikis D, Soulika AM, Mallik B, Klepeis JL, Floudas CA, Lambris JD. Improvement of the anti-C3 activity of compstatin using rational and combinatorial approaches. Biochem Soc Trans 2004; 32:28-32. [PMID: 14748706].
18. Mallik B, Katragadda M, Spruce LA, Carafides C, Tsokos CG, Morikis D, Lambris JD. Design and NMR characterization of active analogues of compstatin containing non-natural amino acids. J Med Chem 2005; 48:274-86. [PMID: 15634022].
19. Katragadda M, Magotti P, Sfyroera G, Lambris JD. Hydrophobic effect and hydrogen bonds account for the improved activity of a complement inhibitor, compstatin. J Med Chem 2006; 49:4616-22. [PMID: 16854067].
20. Morgan BP, Harris CL. Complement, a target for therapy in inflammatory and degenerative diseases. Nat Rev Drug Discov 2015; 14:857-77. [PMID: 26493766].
21. Gorham RD Jr, Forest DL, Tamamis P, Lopez de Victoria A, Kraszni M, Kieslich CA, Banna CD, Bellows-Peterson ML, Larive CK, Floudas CA, Archontis G, Johnson LV, Morikis D. Novel compstatin family peptides inhibit complement activation by drusen-like deposits in human retinal pigmented epithelial cell cultures. Exp Eye Res 2013; 116:96-108. [PMID: 23954241].
22. Gorham RD Jr, Forest DL, Khoury GA, Smadbeck J, Beecher CN, Healy ED, Tamamis P, Archontis G, Larive CK, Floudas CA, Radeke MJ, Johnson LV, Morikis D. New Compstatin Peptides Containing N-Terminal Extensions and Non-Natural Amino Acids Exhibit Potent Complement Inhibition and Improved Solubility Characteristics. J Med Chem 2015; 58:814-26. [PMID: 25494040].
23. Johnson LV, Forest DL, Banna CD, Radeke CM, Maloney MA, Hu J, Spencer CN, Walker AM, Tsie MS, Bok D, Radeke

MJ, Anderson DH. Cell culture model that mimics drusen formation and triggers complement activation associated with age-related macular degeneration. Proc Natl Acad Sci USA 2011; 108:18277-82. [PMID: 21969589].

24. Hu J, Bok D. A cell culture medium that supports the differentiation of human retinal pigment epithelium into functionally polarized monolayers. Mol Vis 2001; 7:14-9. [PMID: 11182021].

25. Maminishkis A, Chen S, Jalickee S, Banzon T, Shi G, Wang FE, Ehalt T, Hammer JA, Miller SS. Confluent monolayers of cultured human fetal retinal pigment epithelium exhibit morphology and physiology of native tissue. Invest Ophthalmol Vis Sci 2006; 47:3612-24. [PMID: 16877436].

26. Yang X, Scott HA, Monickaraj F, Xu J, Ardekani S, Nitta CF, Cabrera A, McGuire PG, Mohideen U, Das A, Ghosh K. Basement membrane stiffening promotes retinal endothelial activation associated with diabetes. FASEB 2016; 30:601-11. [PMID: 26443820].

27. Yang X, Scott HA, Ardekani S, Williams M, Talbot P, Ghosh K. Aberrant cell and basement membrane architecture contribute to sidestream smoke-induced choroidal endothelial dysfunction. Invest Ophthalmol Vis Sci 2014; 55:3140-7. [PMID: 24713480].

28. Ugliengo P, Viterbo D, Chiari G. MOLDRAW - MOLECULAR GRAPHICS ON A PERSONAL-COMPUTER. Z Kristallogr 1993; 207:9-23. .

29. Pettersen EF, Goddard TD, Huang CC, Couch GS, Greenblatt DM, Meng EC, Ferrin TE. UCSF chimera - A visualization system for exploratory research and analysis. J Comput Chem 2004; 25:1605-12. [PMID: 15264254].

30. Janssen BJC, Halff EF, Lambris JD, Gros P. Structure of compstatin in complex with complement component C3c reveals a new mechanism of complement inhibition. J Biol Chem 2007; 282:29241-7. [PMID: 17684013].

31. Brooks BR, Brooks CL, Mackerell AD, Nilsson L, Petrella RJ, Roux B, Won Y, Archontis G, Bartels C, Boresch S, Caflisch A, Caves L, Cui Q, Dinner AR, Feig M, Fischer S, Gao J, Hodoscek M, Im W, Kuczera K, Lazaridis T, Ma J, Ovchinnikov V, Paci E, Pastor RW, Post CB, Pu JZ, Schaefer M, Tidor B, Venable RM, Woodcock HL, Wu X, Yang W, York DM, Karplus M. CHARMM: The biomolecular simulation program. J Comput Chem 2009; 30:1545-614. [PMID: 19444816].

32. Zoete V, Cuendet MA, Grosdidier A, Michielin O. SwissParam: A Fast Force Field Generation Tool for Small Organic Molecules. J Comput Chem 2011; 32:2359-68. [PMID: 21541964].

33. Mohan RR, Gorham RD Jr, Morikis D. A theoretical view of the C3d:CR2 binding controversy. Mol Immunol 2015; 64:112-22. [PMID: 25433434].

34. Tamamis P, Lopez de Victoria A, Gorham RD Jr, Bellows-Peterson ML, Pierou P, Floudas CA, Morikis D, Archontis G. Molecular Dynamics in Drug Design: New Generations of Compstatin Analogs. Chem Biol Drug Des 2012; 79:703-18. [PMID: 22233517].

35. Lopez de Victoria A, Gorham RD Jr, Bellows-Peterson ML, Ling J, Lo DD, Floudas CA, Morikis D. A New Generation of Potent Complement Inhibitors of the Compstatin Family. Chem Biol Drug Des 2011; 77:431-40. [PMID: 21352502].

36. Kang JS, DeLuca PP, Lee KC. Emerging PEGylated drugs. Expert Opin Emerg Drugs 2009; 14:363-80. [PMID: 19453284].

37. Li WJ, Zhan P, De Clercq E, Lou HX, Liu XY. Current drug research on PEGylation with small molecular agents. Prog Polym Sci 2013; 38:421-44. .

38. Risitano AM, Ricklin D, Huang YJ, Reis ES, Chen H, Ricci P, Lin ZE, Pascariello C, Raia M, Sica M, Del Vecchio L, Pane F, Lupu F, Notaro R, Resuello RRG, DeAngelis RA, Lambris JD. Peptide inhibitors of C3 activation as a novel strategy of complement inhibition for the treatment of paroxysmal nocturnal hemoglobinuria. Blood 2014; 123:2094-101. [PMID: 24497537].

39. Sahu A, Kay BK, Lambris JD. Inhibition of human complement by a C3-binding peptide isolated from a phage-displayed random peptide library. J Immunol 1996; 157:884-91. [PMID: 8752942].

40. Morikis D, Lambris JD. Structural aspects and design of low-molecular-mass complement inhibitors. Biochem Soc Trans 2002; 30:1026-36. [PMID: 12440966].

41. Morikis D, Assa-Munt N, Sahu A, Lambris JD. Solution structure of Compstatin, a potent complement inhibitor. Protein Sci 1998; 7:619-27. [PMID: 9541394].

42. Morikis D, Roy M, Sahu A, Troganis A, Jennings PA, Tsokos GC, Lambris JD. The structural basis of compstatin activity examined by structure-function-based design of peptide analogs and NMR. J Biol Chem 2002; 277:14942-53. [PMID: 11847226].

43. Sahu A, Soulika AM, Morikis D, Spruce L, Moore WT, Lambris JD. Binding kinetics, structure-activity relationship, and biotransformation of the complement inhibitor compstatin. J Immunol 2000; 165:2491-9. [PMID: 10946275].

Articles are provided courtesy of Emory University and the Zhongshan Ophthalmic Center, Sun Yat-sen University, P.R. China. The print version of this article was created on 26 October 2016. This reflects all typographical corrections and errata to the article through that date. Details of any changes may be found in the online version of the article.